Materials and Design 195 (2020) 109073

Contents lists available at ScienceDirect

Materials and Design

journal homepage: www.elsevier.com/locate/matdes

The incorporation of graphene to enhance mechanical properties of polypropylene self-reinforced polymer composites

Jian Wang [a,b,*], Feiyan Song [c], Yongzhi Ding [c], Mingwang Shao [c]

[a] College of Mechanical and Electrical Engineering, Beijing University of Chemical Technology, Beijing 100029, China
[b] State Key Laboratory of Organic-Inorganic Composites, Beijing University of Chemical Technology, Beijing 100029, China
[c] School of Chemistry and Chemical Engineering, Beijing Institute of Technology, Beijing 100081, China

HIGHLIGHTS

- Polypropylene/graphene platelets single-polymer composites (PP/GNP SPC) were prepared.
- Compared with pure PP, 117% and 116% increases of tensile strength and modulus were obtained by the PP/0.062 wt% GNP SPC.
- Compared with PP SPCs, 116% increase of interfacial strength was obtained by the PP/0.062 wt% GNP SPC.
- Graphene nanotechnology and self-reinforced mechanism enhanced the mechanical properties of the PP/GNP SPC.

GRAPHICAL ABSTRACT

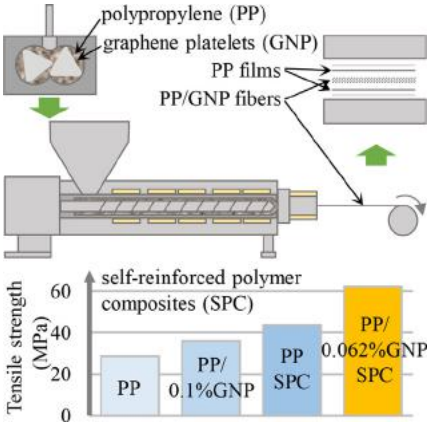

ARTICLE INFO

Article history:
Received 7 May 2020
Received in revised form 17 August 2020
Accepted 17 August 2020
Available online 19 August 2020

Keywords:
Self-reinforced polymer composites
Graphene
Melt spinning
Film stacking
Mechanical properties

ABSTRACT

Lightweight, easy recyclability and improved bonding can be achieved by self-reinforced polymer composites (SPC). However, the mechanical properties of SPC are usually limited. This paper describes the incorporation of graphene platelets (GNP) into polypropylene (PP) to produce PP/GNP SPC. PP/GNP fibers were firstly prepared by melt compounding and spinning, and then PP/GNP SPC were produced by film stacking. The thermal, mechanical, and morphological properties of the produced samples were characterized via DSC, WAXD, tensile test, peeling test, optical microscopy, and SEM. The combination of film stacking technology of SPC and nanotechnology of graphene enhanced the mechanical properties significantly. The tensile strength, tensile modulus, and interfacial strength of PP SPC with only 0.062 wt% GNP were increased by 117, 116, and 116%, respectively. The reinforcement is attributed to the high intrinsic mechanical properties of GNP and the self-reinforced mechanism. The spinning promotes the alignment of GNP, and the compaction process induces the in-plane orientation of GNP. In addition, a small number of GNP do not increase the cost significantly.

1. Introduction

Self-reinforced polymer composites (SPC), whose reinforcement and matrix phase come from the same polymer or the same polymer type [1], are also called "single-polymer composites", "homocomposites", or "all-polymer composites". SPC have attracted the attention of academia

* Corresponding author at: 15 Beisanhuan East Road, Chaoyang, Beijing 100029, PR China.
E-mail address: wjj_0107@163.com (J. Wang).

https://doi.org/10.1016/j.matdes.2020.109073

and industry and will continue to be the focus of attention due to the strong adhesion between matrix and reinforcement, reduced weight, and enhanced end-life recyclability [2–5]. At present, SPC parts are mostly used in automotive, sport/leisure sectors, industrial cladding, building, and construction [4]. Different thermoplastic polymers can be used to manufacture SPC [2,3], including polyethylene (PE), polypropylene (PP), polyethylene terephthalate (PET), polyethylene naphthalate (PEN), polyamide (PA), polylactic acid (PLA), polymethylmethacrylate (PMMA), polytetrafluoroethylene (PTFE), polyvinyl alcohol (PVOH) [6], and liquid-crystalline copolyesters [7]. The new members of the SPC family, micro-, nanofibrillar SPC [8], and microcellular SPC foams [9,10] have been developed. Research activities on SPC target the new materials [11–13], novel preparation technologies [14–16], productivity [17–20], and multifunctionality [4,21–24]. The major challenge in the fabrication of SPC is to establish a processing temperature window due to the small melting temperature difference between the fiber and the matrix [2,3,5]. The mechanical properties of SPC are usually limited by the processing temperature and the fiber fraction. Fibers melt easily at a higher temperature, whereas lower temperatures cause weak adhesion in the fiber/matrix interface. The incorporation of nanoparticles to enhance the properties of SPC has become an issue of concern to the academic community. Hine et al. [25] investigated the incorporation of carbon nanofibers (CNF) in PP SPC. When the content of filler increased to 4 wt%, the Young's modulus of PP/CNF SPC increased to about 140%. Foster et al. [26] incorporated talc-filled interleaved films in the hot compaction of PP SPC to investigate the enhancement effect of interfacial bonding. It demonstrated that the interlayer adhesion of hot compacted SPC could be improved with a number of different fillers in addition to CNF. The hybridisation with SPC is another promising strategy to modify the mechanical properties [27,28]. Hybrid carbon fiber/PP SPC [29,30], hybrid carbon fiber/PA12 SPC [31], and steel fiber/PP SPC [32] were developed and investigated gradually.

Graphene, following fullerene and carbon nanotubes (CNT), has attracted great attention [33]. Due to the unique structure, graphene has high Young's modulus (~1100 GPa), high fracture strength (~125 GPa), and excellent electrical and thermal conductivity. The superior properties of graphene compared to polymers are seen in polymer/graphene nanocomposites [34]. It has been suggested that the incorporation of a small amount of graphene can significantly improve polymer's properties, especially the mechanical properties [35]. In addition, the polymer/graphene nanocomposites have much better mechanical and electrical properties in comparison to the clay or other carbon filler-based polymer nanocomposites [34,36,37].

No study to this date has investigated the incorporation of graphene into SPC to prepare graphene-based SPC. The purpose of this paper is to combine a small quantity of graphene platelets (GNP) into PP and then prepare graphene-reinforced PP SPC with enhanced mechanical properties. The small number of GNP will not increase the cost a lot but can improve processing conditions as well as the mechanical properties of the final part. The combination of melt compounding, melt spinning, and film stacking was used for the preparation of the samples. The effect of graphene was regarded in the investigation. Tensile test, DSC, peeling test, WAXD, and SEM were conducted for the characterization of different samples.

2. Experimental

2.1. Materials

PP pellets (Marlex HGZ—1200, Phillips Sumika Polypropylene Company, LLC, Woodlands, USA) with a density of 0.907 g/cm^3 and a melt flow index (MFI) of 115 g/10 min at 230 °C were used. Graphene platelets (GNP) were purchased from the Sixth Element Materials Technology Co. Ltd. (Changzhou, China). The graphene had an apparent density of 56 mg/ml, a specific surface area of 211 m^2/g, and a particle size of 4.69 μm. The number of layers in the GNP was two to ten.

2.2. Compounding

Fig. 1 presents the schematic of the preparation process for the PP/GNP SPC. A 50 ml twin-screw compounder (HAPRO RM200, Changchun Intelligence Instrument Co., Ltd., China) was used in the compounding process. PP pellets with different content of GNP (0.01, 0.02, 0.05, and 0.1 wt%) were mixed at 200 °C for 5 min with the screw speed of 30 rpm, and then the screw speed was increased to 100 rpm and the compounding time was 15 min. Finally, the PP/GNP composites were removed and granulated.

2.3. Melt spinning

The prepared PP/GNP composite pellets were added into a single-screw extruder (HAPRO RM200, Changchun Intelligence Instrument Equipment Co., Ltd., China) to fabricate PP/GNP fibers. A capillary with

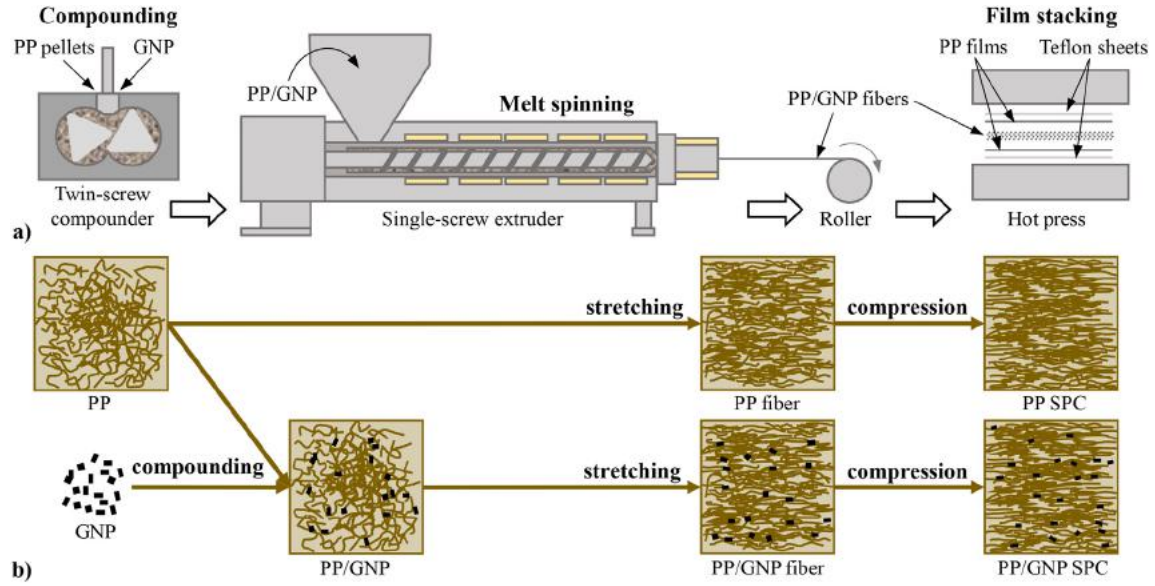

Fig. 1. Schematic of the preparation process for the PP/GNP SPC (a) and the morphology transformation of materials during the process (b).

a length of 10 mm and a diameter of 1 mm was used for the melt spinning. The diameter of the spinning roller was 90 mm. The distance between the spinning roller and the capillary was 650 mm. In order to investigate the influence of processing conditions, different melt spinning temperatures of 180, 190, 200, 210, 220, and 230 °C, and different roller speeds of 80, 120, 160, and 200 rpm were used. Pure PP fibers were also prepared for comparison.

2.4. Film stacking

Pure PP films were first prepared by using a hot press (BP-8107-D-100, Baopin Precision Instrument Co., Ltd., China) at 170 °C. The fibers were aligned unidirectionally between two films, and the laminates were placed between two Teflon sheets and pressed. The fiber volume fraction was 62.1% for the PP SPC. The compaction pressure was 2 MPa. The PP SPC samples were prepared at different compaction temperatures ranged 155–170 °C for different compaction time ranged 100–120 s to obtain an optimum condition. Then 160 °C and 110 s were used in the following film stacking to prepare the PP/GNP SPC with different GNP content. For comparison, PP/GNP films were also prepared at 170 °C for 100 s.

2.5. Mechanical tests

The tensile properties of the prepared fibers and the composites were tested by using a universal testing machine (XWW-20KN, Beijing Jinshengxin Testing Machine Co., Ltd., China). The standard test method of ASTM D3822 was used for the prepared fibers. The length of the pre-test sample was 10 cm, and the crosshead speed was 150 mm/min. For the composites, the pre-tested samples were cut down into the geometry with a length of 75 mm and a width of 5 mm according to the ISO 527-2 type 1BA standard. The crosshead speed was 5 mm/min. All tensile tests were performed under room conditions.

The universal testing machine was also used for the T-peel test to determine the interfacial strength of the PP/GNP SPC. During the film stacking, an additional Teflon film was employed in the middle of the specimen to create an unbonded region for the T-peel test. The specimens, 10 mm wide and 100 mm long, were tested at a crosshead speed of 20 mm/min and at room temperature. The 10 mm long unbonded ends were bent apart for clamping in the grips of the testing machine. T-peel tests were carried out along the parallel fiber directions. The peel strength was calculated in a displacement range from 30 to 70 mm.

2.6. Differential scanning calorimetry (DSC)

A differential scanning calorimeter (TA Q200, TA Instruments, New Castle, USA) was applied to study the thermal properties. The samples were heated from 40 °C to 200 °C with a rate of 10 °C/min and held for 10 min at 200 °C to erase the thermal and mechanical history, and then cooled to 40 °C with the rate of 10 °C/min in N_2 atmosphere. The degree of crystallinity (X_c) was determined by the following equation:

$$X_c = \frac{1}{1-W_f} \times \frac{\Delta H_m}{\Delta H_m^0} \times 100\% \quad (1)$$

where W_f is the weight fraction of GNP, ΔH_m is the melting enthalpy, ΔH_m^0 is the melting enthalpy of PP in 100% crystalline state and 190 J/g was used [38].

2.7. Wide-angle X-ray diffraction (WAXD)

Wide-angle X-ray diffraction (WAXD) patterns of the samples were tested in the Bruker D8 Advance (Germany) with CuK_α radiation ($\lambda = 0.154$ nm). Scanning was conducted in a range of 5° to 35° with a speed of 1°/min. The voltage was 40 kV and the current was 40 mA.

2.8. Microscopy

An optical microscope (XSP-8CA, Shanghai Optical Instrument Factory, China) was used to observe the morphology of the samples. A scanning electron microscope (SEM, Nanonova 230; FEI, Hillsboro, OR, USA) was used to observe the fracture surface of the PP/GNP SPC with an accelerating voltage of 25 kV. The fractured section of the sample was gold coated.

3. Results and discussion

3.1. Morphology

The optical microscope images of the PP/GNP fibers prepared at different process conditions are shown in Fig. 2. It is noted that some of the large blurred black dots are dust. The effects of the roller speed, spinning temperature and graphene concentration can be observed. The fiber diameter decreases with increasing roller speed and spinning temperature. More GNP can be seen in the fibers with higher graphene concentration. The GNP uniformly dispersed in the fibers, which demonstrates the effective compounding. It also indicates that the spinning process benefits the alignment of GNP.

The optical microscope images of the PP/GNP fibers prepared at different process conditions are shown in Fig. 3. Some vertical stripes in the images are due to the roughness surface of the mold plate, and some small black dots are dust. Fig. 3 (a) shows the PP SPC prepared at different compaction temperature. The direction of the fiber orientation in the PP SPC can be observed. Obvious interfaces between fibers can be seen at the compaction temperature of 155 °C, indicating poor interface bonding. The interface becomes more blurred in the PP SPC prepared at higher compaction temperature. There is no clear interface at 170 °C, indicating more fibers were melted. Fig. 3 (b) shows the PP/GNP SPC with different graphene concentration. The addition of GNP has

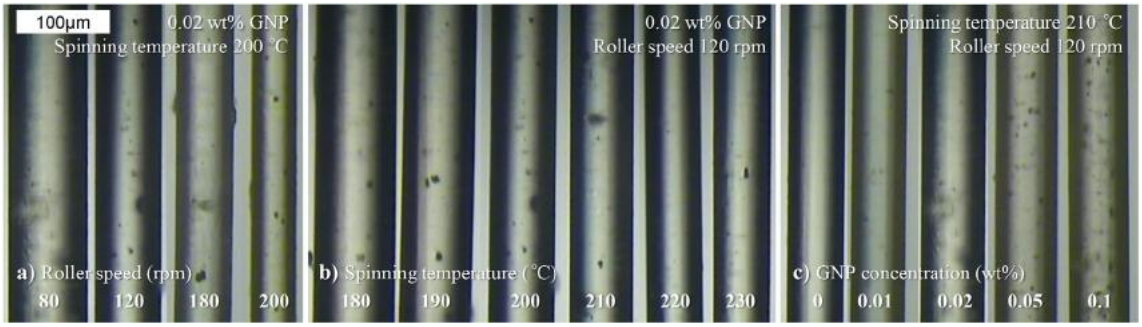

Fig. 2. Optical microscope images of the PP/GNP fibers prepared at different process conditions: roller speed (a), spinning temperature (b), and graphene concentration (c).

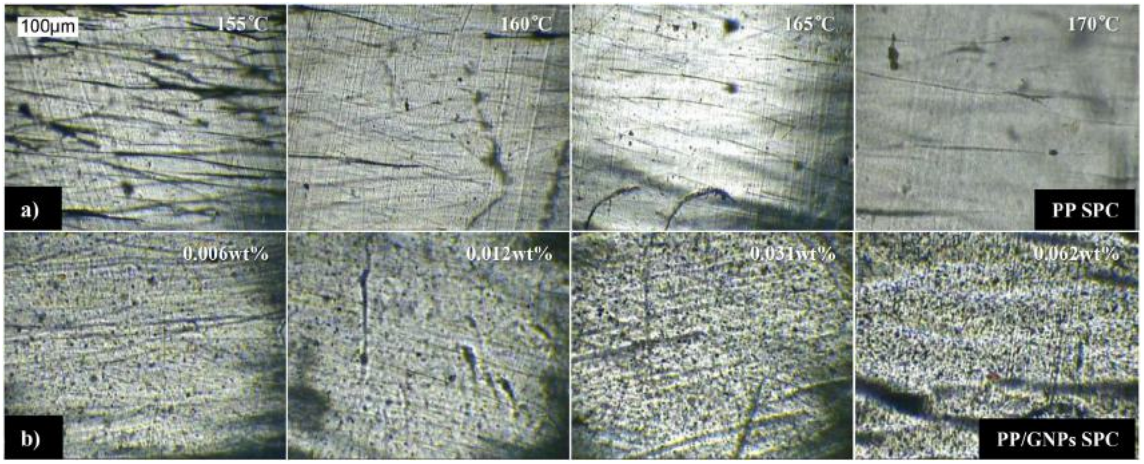

Fig. 3. Optical microscope images of the PP SPC prepared at different compaction temperature (a) and the PP/GNP SPC with different graphene concentration (b).

affected the transparency of the sample. Good dispersion of GNP can be seen, and more GNP can be found in the PP/GNP SPC with higher graphene concentration.

Fig. 4 (a) shows the tensile fracture section of the PP/0.031 wt% GNP SPC. Some surface layers of fibers were destroyed and microfibrillation occurred. Some debonding and bonding interfaces between the fibers and the matrix can be seen, indicating the stress was transmitted to the fiber through the interface of the matrix during the tensile test. Fig. 4 (b) and (c) present the fracture section of the PP/0.006 wt% GNP SPC and the PP/0.031 wt% GNP SPC after the peeling test, respectively. The fiber orientation on the tear surface is obvious in the images with low magnification, but the intertwined fibers can also be seen. The intertwined fiber layout decreases the ability of fibers to bear the tensile force and affects the penetration of the matrix. There are many matrix particles attached on the surface of fibers, indicating good interfacial adhesion between the fibers and the matrix. Several large parts of matrix exist between fibers, indicating the matrix has impregnated the fiber filaments during the film stacking. Some fibers were deformed and a certain degree of microfibrillation occurred, which further indicates good interfacial properties. In some images with high magnification, the GNP can be observed. The yellow arrows indicate the presence of some GNP. The GNP appears on the fiber surfaces, indicating that the interface between fibers was partially fused during the film stacking and some GNP moved to the interface due to the transfer of heat and force.

3.2. DSC

Fig. 5 shows the DSC thermograms of PP matrix, PP fiber, and PP/GNP fiber. The melting temperature (T_m), melting enthalpy (ΔH_m), and degree of crystallinity (X_c) are summarized in Table 1. PP can form α, β, and γ crystal structures at different crystallization conditions. The α-monoclinic crystal is the most common and stable crystal structure that can be easily

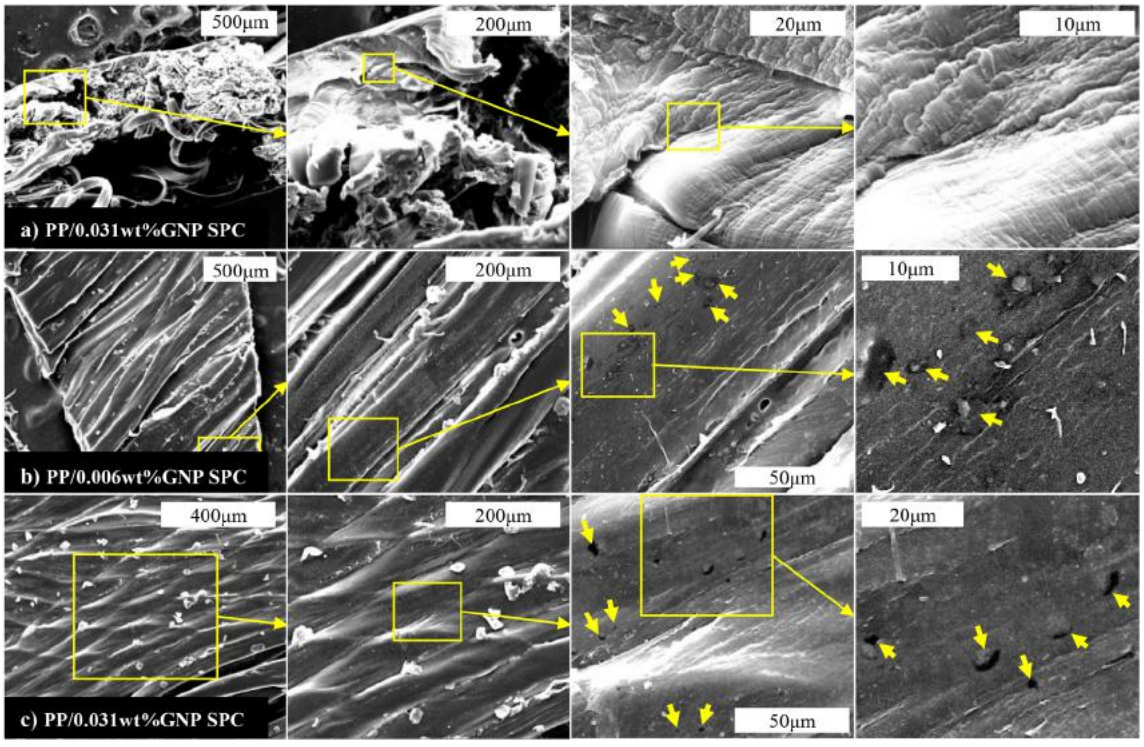

Fig. 4. Scanning electron microscope images of the PP/GNP SPC: tensile fracture section of the PP/0.031 wt% GNP SPC (a), peel fracture section of the PP/0.006 wt% GNP SPC (b), and peel fracture section of the PP/0.031 wt% GNP SPC (c).

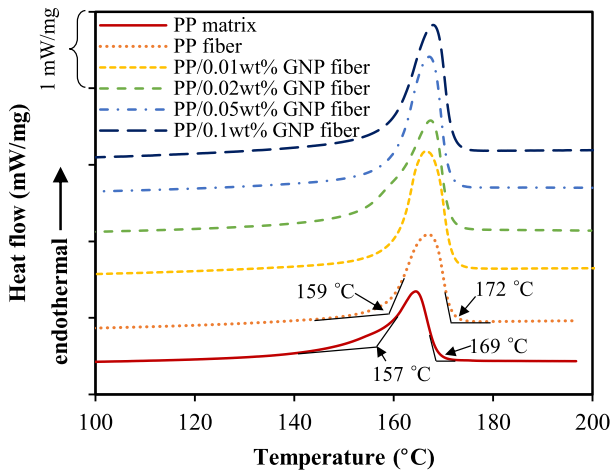

Fig. 5. DSC thermograms of PP matrix, PP fiber, and PP/GNP fiber.

Table 1
DSC data of PP matrix, PP fiber, and PP/GNP fiber.

Sample	T_m (°C)	$\triangle H_m$ (J/g)	X_c (%)
PP matrix	164.4	70.6	37.2
PP fiber	167.0	81.8	43.1
PP/0.01 wt% GNP fiber	166.6	98.8	52.0
PP/0.02 wt% GNP fiber	167.4	99.3	52.3
PP/0.05 wt% GNP fiber	167.2	101	53.5
PP/0.1 wt% GNP fiber	168.0	103	54.3

obtained under normal processing conditions. As shown in Fig. 5, each sample has only one melting peak, indicating that only the α crystal structure exists. Compared with the PP matrix, the melting temperatures of the pure PP fiber and the PP/GNP fiber were higher, indicating that the molecular chain of PP was stretched during the melt spinning and the fibers were easily oriented in the direction of the stretching axis. There is no significant difference in the melting temperatures between the pure PP fiber and the PP/GNP fiber. The melting temperature slightly increases with the increase of graphene concentration. The degree of crystallinity of the fibers is higher than that of the PP matrix, and the crystallinity degree of the PP/GNP fiber increases with increasing graphene concentration. Some literature [39,40] has presented that the GNP acts as a barrier to the formation of large crystallites and restricts the polymer chain movements, thus the crystallinity would be decreased. However, in this study, the graphene size was small and the concentration was low. The GNP acts as a seed for heterogeneous nucleation, thus crystallization can be facilitated [41]. Furthermore, the GNP can provide more chances for more molecular chains to form crystalline structures, and the attraction forces along a chain could be lower in the presence of a "physical wall" like the GNP, which leads to much higher mobility hence favoring crystallinity [42].

In the film stacking of SPC, the compaction temperature allows polymer matrix and the reinforcement fibers melting partially so that the matrix and the reinforcement can be organically combined, which is critical for the preparation of SPC. As shown in Fig.5, the PP matrix begins to melt at 157 °C and melts completely at 169 °C. The melting point of the matrix is 164.7 °C. However, the PP fiber begins to melt at 159 °C and melts completely at 172 °C, and it has a melting point of 167 °C. Therefore, the temperature ranged from 155 to 170 °C was chosen as the compaction temperature.

3.3. WAXD

The WAXD patterns of pure PP matrix, pure PP fiber, PP/0.05 wt% GNP fiber, PP SPC, and PP/0.031 wt% GNP SPC are shown in Fig. 6. The PP matrix has seven diffraction peaks of 14.1°,16.9°, 18.6°, 22.1°,

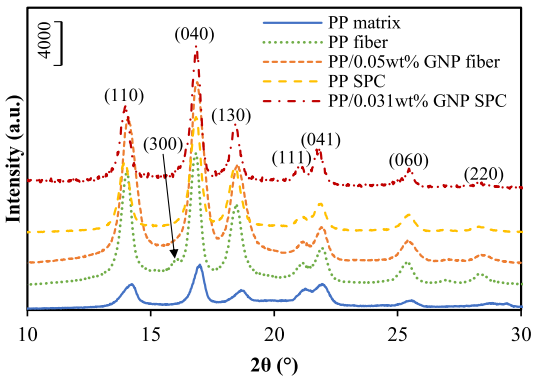

Fig. 6. WAXD patterns of PP matrix, PP fiber, PP/0.05 wt% GNP fiber, PP SPC, and PP/0.031 wt% GNP SPC.

21.8°, 25.5°, and 28.8°, corresponding to the (110), (040), (130), (111), (041), (060), and (220) crystal planes, respectively. These peaks correspond to the α-monoclinic crystal structure. The PP fiber has the same diffraction peak as the PP matrix, but the intensity of the diffraction peak is remarkably enhanced. It is because the molecular chain of PP had an obvious orientation during the melt spinning and the crystallinity was improved. Further, the (300) plane of β-crystals appears for the PP fiber, but the number of β-crystals is insignificant. The crystal types of the PP/0.05 wt% GNP fiber does not change, still being α-monoclinic. However, the intensity of diffraction peaks of the PP/0.05 wt% GNP fiber is stronger than that of the PP fiber. This illustrates that the presence of graphene promoted fiber orientation and crystallization. The crystal shapes of the PP SPC and the PP/GNP SPC have not changed, and the intensity of diffraction peaks is between the matrix and the fiber. This indicates that the fiber has a good reinforcing effect on the composites. In comparison with the PP SPC, the intensity of diffraction peaks of the PP/GNP SPC is stronger. The GNP exerts a considerable nucleating effect on the crystallization of PP by inducing particular planes, such as (110), (040), (111), (041), which can be formulated by the epitaxial growth of polymer chains on the GNP. Compared with the PP/0.05 wt% GNP fiber, the peak positions for the PP/0.031 wt% GNP SPC are decreased. This indicates that the addition of PP matrix to the PP/0.05 wt% GNP fibers caused a decrease in the degree of crystallinity. The diffraction peak of the graphene is not observed because of the small number of GNP, but it indicates that GNP were successfully dispersed.

3.4. Tensile properties

Fig. 7 shows the tensile properties of the PP/GNP fibers prepared at different process conditions. The maximum values of tensile strength and modulus for the PP/0.02 wt% GNP fiber can be obtained by using the spinning temperature of 210 °C and the roller speed of 120 rpm. The tensile strength and modulus increase and the elongation at break decrease with increasing graphene content. The tensile strength and modulus of the PP/0.1 wt% GNP fiber were 179.3 ± 9.1 MPa and 8.05 ± 1.1 GPa, 1.64 times and 1.73 times than those of pure PP fiber, respectively. This indicates that the addition of a small amount of graphene can greatly improve the mechanical properties of polymer fibers. Graphene agglomerates when much higher content is used, which decreases the mechanical properties of the composite materials. In this paper, the tensile strength and modulus of fibers did not decrease because the content of graphene was very low. It demonstrates the good dispersion of the graphene in the polymeric matrix.

Fig. 8 (a) illustrates the effect of the compaction temperature on the tensile properties of the PP SPC. The tensile strength and modulus of the PP SPC increased first and then decreased with the increase of the

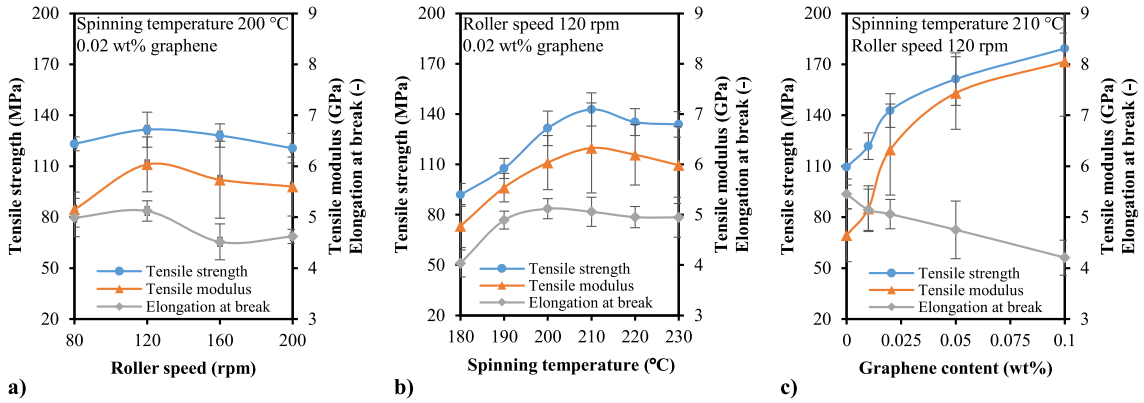

Fig. 7. Tensile properties of the PP/GNP fibers prepared at different process conditions: roller speed (a), melt spinning temperature (b), and graphene content (c).

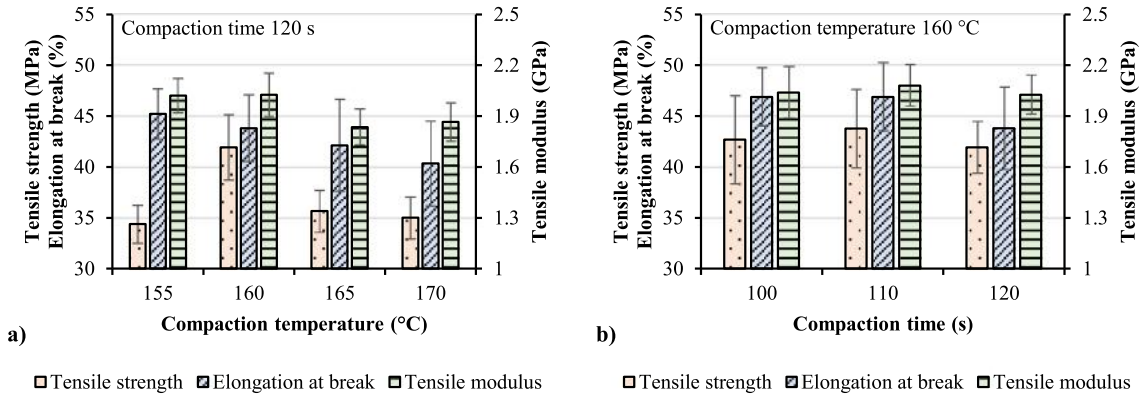

Fig. 8. Tensile properties of the PP SPC prepared at different compaction temperature (a) and compaction time (b).

compaction temperature. According to the onset melting temperatures of the PP matrix and fiber (157 and 159 °C), the PP matrix and fibers were partially melted at the compaction temperature of 160 °C. Macromolecules move and polymer chains rearrange as the melting temperature is approached. The partially melted material recrystallizes to bind the structure together and fill the interstitial voids, which improves the mechanical properties. However, the crystallinity of the PP SPC will decrease due to the penetration of the matrix, which reduces the mechanical properties. The PP matrix and fibers could be compacted together under the constant pressure to form PP SPC. The tensile strength and modulus of pure PP were 28.62 ± 1.2 MPa and 1.19 ± 0.2 GPa, respectively. The maximum tensile strength and modulus of the PP SPC were 41.97 ± 3.19 MPa and 2.14 ± 0.12 GPa, about 1.47 times and 1.80 times as high as that of the pure PP, respectively. The mechanical properties of the composites decreased at higher temperatures of 165 and 170 °C because of more fiber melting. Therefore, the compaction temperature of 160 °C was chosen as the optimum temperature for the film stacking. In addition, the compaction time is also a significant factor to prepare SPC [43]. Fig. 8 (b) presents the effect of the compaction time on the tensile properties of the PP SPC. The interfacial bonding between the fiber and the matrix is poor at a short compaction time, while longer compaction time will cause the composite material to be overheated and more fiber melting. The tensile strength and modulus of the PP SPC had the optimal values of 43.79 ± 3.85 MPa and 2.08 ± 0.12 GPa, respectively, when the compaction temperature of 160 °C and the compaction time of 110 s were used. Additionally, higher compaction temperature and longer compaction time led to lower elongation at break.

The tensile properties of the PP/GNP films and the PP/GNP SPC are shown in Fig. 9. As the graphene concentration increased, the tensile strength and modulus increased, and the elongation at break decreased. The homogeneous dispersion of nanoparticles in the polymer matrix is one of the key factors to enhance the mechanical properties of the polymer composites. The aggregation of nanoparticles will lead to structural defects in composite materials and thus affect the mechanical properties. There was no decrease in the tensile strength and modulus, indicating the GNP dispersed homogeneously. The maximum tensile strength and modulus of the PP/GNP film were 36.03 ± 0.9 MPa and 2.7 ± 0.2 GPa, respectively. A 25.9% enhancement for the tensile strength of the PP/GNP film was observed with the incorporation of 0.1 wt% GNP. This indicates the attribution of high intrinsic mechanical characteristics of graphene. The maximum tensile strength and modulus of the PP/0.062 wt% GNP SPC were 62.18 ± 6.18 MPa and 2.57 ± 0.16 GPa, respectively. Compared with pure PP, the addition of only 0.062 wt% of GNP into PP SPC resulted in increases of tensile strength and modulus of 117% and 116%, respectively. Compared with the PP SPC without GNP, an increase in the tensile strength of 42% was achieved. This indicates the importance of the incorporation of graphene in the improvement of mechanical properties. The enhanced tensile strength is attributed to the large aspect ratio and high intrinsic mechanical characteristics of graphene and the relatively strong interfacial interaction between the PP and graphene. Furthermore, compared with PP/0.1 wt% GNP films, a 73% enhancement for tensile strength was obtained by the PP/0.062 wt% GNP SPC. This demonstrates that the strength of PP/GNP composites was further improved in cooperation with the excellent bonding properties of the SPC prepared by the spinning and film stacking processes. The schematic description of the morphology transformation of materials during the process is shown in Fig. 1 (b). The spinning of PP/GNP fibers benefits the orientation of molecular chains. GNP can also be dragged by PP chains resulting in their orientation along the stretching direction. Moreover, the film stacking process on

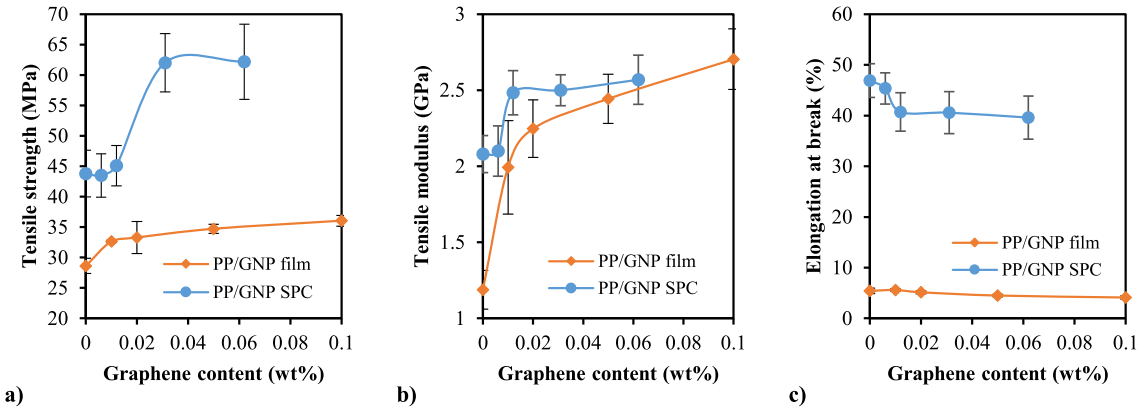

Fig. 9. Tensile properties of the PP/GNP films and the PP/GNP SPC with different graphene content: tensile strength (a), tensile modulus (b), and elongation at break (c).

Table 2
Comparison of the tensile strength and modulus of PP/GNP SPC with other PP/graphene composites from literature.

Graphene type	Preparation method	Graphene content	Increase in tensile		Ref.
			strength	modulus	
graphene nano-platelets (GNP)	melt compounding, spinning, and film stacking	0.062 wt%	117%	116%	this study
three types of GNP	melt compounding and injection molding	5 wt%	17.5%	28.3%	[41]
three types of GNP	melt compounding and injection molding	0.5 wt%	5%	98%	[46]
GNP	melt compounding and injection molding	10 wt%	−12%	54%	[47]
graphene nano-sheets (GNS)	melt compounding and hot press	1 wt%	−11%	19%	[48]
GNS	in situ polymerization	17.4 wt%	25%	50%	[49]
graphite oxide (GO)	melt-blending the coated graphene with PP matrix	0.42 vol%	75%	74%	[50]
alkylated graphene oxide (AGO)	ultrasonicated xylene and stirring	0.1 wt%	−5%	70%	[51]
graphite particles	solid-state shear pulverization	2.7 wt%	60%	100%	[52]

the unidirectional PP/GNP fibers can further induce the in-plane orientation of GNP. Additionally, temperature is the key factor in the production of SPC [44]. The thermal analysis indicates that the melting temperature of PP/GNP fibers increased a little as the number of GNP increased, which can prevent fibers from melting and thus enlarge the processing temperature window [2,3].

The tensile modulus of the PP/GNP SPC increased with increasing graphene content but it was not much higher than that of the PP/GNP film. The main reason is the thickness dependence of the film. The average thickness of the PP/GNP films was 0.1365 mm, while the average thickness of the PP/GNP SPC was 0.3614 mm. The modulus of elasticity values of polymers in the tensile test decreases when the specimen thickness increases in the range 0.1–2 mm [45]. It is not the consequence of morphological changes and is independent of the way by which the modulus of elasticity is measured [45]. Much lower elongations at break for the PP/GNP films compared to the PP/GNP SPC, as shown in Fig. 9 (c), indicate the significant effect of the thickness.

Table 2 shows significant enhancements of tensile strength and modulus of the PP/GNP SPC in comparison with other PP/graphene nanocomposites from literature [41,46–52]. This comparison is rough because it does not take differences in material types, especially the different types and sizes of graphene, into account. However, it indirectly indicates the superiority of the combination between the graphene technology and the self-reinforcing mechanism to improve the mechanical performance of polymer composites.

3.5. Interfacial properties

In order to clearly know the mechanism of the graphene in the improvement of the interfacial properties of the PP SPC, the interfacial adhesion was evaluated by measuring the peeling force. Fig. 10 shows curves of the peeling force as a function of peeling displacement for

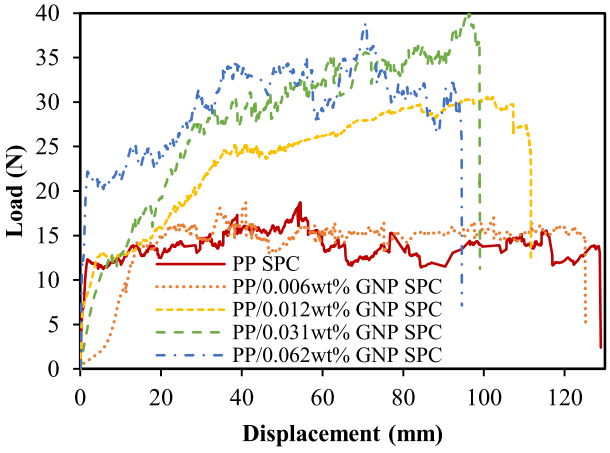

Fig. 10. Peel force as a function of displacement for the PP/GNP SPC with different graphene content.

the PP/GNP SPC with different graphene content. The addition of 0.006 wt% GNP did not significantly improve the interfacial strength. With the increase of graphene content, the peeling force increased. When the graphene content increased to 0.062 wt%, the average peeling force was 32.4 N which is significantly higher than the average peeling force of 15 N of the PP SPC without GNP. A 116% increase in the interfacial strength has been achieved. This indicates that the presence of graphene has effectively enhanced the interfacial properties. It can be confirmed that a strong interfacial interaction between the GNP and PP has been realized. Moreover, some GNP could be transferred to the interface between the fibers during the film stacking, which further

improved the interfacial adhesion. Additionally, the displacement at the time of peeling failure was shorter when the graphene content was higher. This indicates that the peeling failed earlier since the interfacial properties of the PP/GNP SPC were further enhanced.

4. Conclusion

The PP/GNP SPC with different content (up to 0.1 wt%) of GNP were prepared by the combined processes including compounding, melt spinning and film stacking. The effects of graphene on thermal, mechanical, and interfacial properties of the composites were analyzed. The melting temperatures and crystallinity of the PP/GNP fiber increased as the number of GNP increased, indicating that the GNP acts as a nucleating agent. The mechanical properties of PP/GNP fibers and PP/GNP films also increased with increasing graphene content, indicating an efficient load transfer between the GNP and PP matrix. Combined with the technology of SPC, the tensile strength of the PP/GNP SPC was improved to 62.18 ± 6.18 MPa. The addition of only 0.062 wt% of GNP resulted in a substantial increase of the tensile strength of about 117%, 73%, and 42% as compared with the tensile strength of the pure PP, PP/0.1 wt% GNP film, and PP SPC, respectively. The elongation to failure of composites decreased with the addition of GNP. The average peeling force of the PP/0.062 wt% GNP SPC was 32.4 N, a 116% enhancement was obtained compared to the PP SPC. Optical microscopy and SEM were used to observe the PP/GNP fibers and the PP/GNP SPC and illustrated a good dispersion of GNP.

This work gives an effective strategy to produce PP/GNP SPC. The addition of GNP with high intrinsic mechanical characteristics can enhance the mechanical properties of the polymer and simultaneously improve the interfacial properties of the SPC. The melt compounding can confirm the dispersion of GNP and the interfacial interaction between GNP and PP chains. The melt spinning can lead to the orientation of molecular chains and GNP in the hot stretching axis. The film stacking can confirm the interfacial adhesion between PP fibers, enhance the interfacial interaction between GNP and PP matrix, and induce the in-plane orientation of GNP.

Data availability statement

The raw/processed data required to reproduce these findings are available to download from [doi:10.17632/5ys9dmmcck.2].

Declaration of Competing Interest

The authors declare that they have no known competing financial interests or personal relationships that could have appeared to influence the work reported in this paper.

Acknowledgements

The project was financed by the National Natural Science Foundation of China (Project No. 51873021). We thank Mr. Cemi Kahve for helping to modify the language.

References

[1] N.J. Capiati, R.S. Porter, The concept of one polymer composites modelled with high density polyethylene, J. Mater. Sci. 10 (1975) 1671–1677.
[2] K.P. Matabola, A.R.D. Vries, F.S. Moolman, A.S. Luyt, Single polymer composites: a review, J. Mater. Sci. 44 (2009) 6213–6222.
[3] J. Karger-Kocsis, T. Bárány, Single-polymer composites (SPCs): status and future trends, Compos. Sci. Technol. 92 (2014) 77–94.
[4] C. Gao, L. Yu, H. Liu, L. Chen, Development of self-reinforced polymer composites, Prog. Polym. Sci. 37 (2012) 767–780.
[5] J. Wang, Polypropylene single-polymer composites, in: P.M. Visakh, P. Matheus (Eds.), Polypropylene-Based Biocomposites and Bionanocomposites, John Wiley & Sons 2017, pp. 177–246.
[6] A. Dorigato, A. Pegoretti, Biodegradable single-polymer composites from polyvinyl alcohol, Colloid Polym. Sci. 290 (4) (2012) 359–370.
[7] A. Pegoretti, A. Zanolli, C. Migliaresi, Preparation and tensile mechanical properties of unidirectional liquid crystalline single-polymer composites, Compos. Sci. Technol. 66 (2006) 1970–1979.
[8] S. Fakirov, Nano−/microfibrillar polymer–polymer and single polymer composites: the converting instead of adding concept, Compos. Sci. Technol. 89 (2013) 211–225.
[9] J. Wang, D. Chen, Microcellular polypropylene single-polymer composites prepared by insert-microcellular injection molding, Compos. A 90 (2016) 567–576.
[10] J. Wang, D. Chen, Flexural properties and morphology of microcellular-insert injection molded all-polypropylene composite foams, Compos. Struct. 187 (2018) 403–410.
[11] C. Gao, L. Meng, L. Yu, G.P. Simon, H. Liu, L. Chen, S. Petinakis, Preparation and characterization of uniaxial poly(lactic acid)-based self-reinforced composites, Compos. Sci. Technol. 117 (2015) 392–397.
[12] L. Tong, P. Zheng, H. Tang, K. Jia, X. Liu, Novel high-temperature-resistant single-polymer composites based on self-reinforced phthalonitrile end-capped polyarylene ether nitrile, Mater. Lett. 159 (2015) 337–340.
[13] L. Han, H. Xu, X. Sui, L. Zhang, Y. Zhong, Z. Mao, Preparation and properties of poly(ε-caprolactone) self-reinforced composites based on fibers/matrix structure, Inc. J. Appl. Polym. Sci. 134 (2017) 44673.
[14] S.D. Tohidi, A.M. Rocha, N.V. Dencheva, Z. Denchev, Single polymer laminate composites by compression molding of knitted textiles and microparticles of polyamide 6: preparation and structure-properties relationship, Compos. A 109 (2018) 171–183.
[15] D. Hofmann, A. Kurek, R. Thomann, J. Schwabe, S. Mark, M. Enders, T. Hees, R. Mülhaupt, Tailored nanostructured HDPE wax/UHMWPE reactor blends as additives for melt-processable all-polyethylene composites and in situ UHMWPE fiber reinforcement, Macromolecules 50 (2017) 8129–8139.
[16] T. Hees, F. Zhong, C. Koplin, R. Jaeger, R. Mülhaupt, Wear resistant all-PE single-component composites via 1D nanostructure formation during melt processing, Polymer 151 (2018) 47–55.
[17] J. Wang, S. Wang, D. Chen, Development and characterization of insert injection moulded polypropylene single-polymer composites with sandwiched woven fabric, Compos. Sci. Technol. 117 (2015) 18–25.
[18] J. Andrzejewski, P. Przyszczypkowski, M. Szostak, Development and characterization of poly(ethylene terephthalate) based injection molded self-reinforced composites. Direct reinforcement by overmolding the composite inserts, Mater. Des. 153 (2018) 273–286.
[19] J. Jiang, X. Liu, M. Lian, Y. Pan, Q. Chen, H. Liu, G. Zheng, Z. Guo, D.W. Schubert, C. Shen, C. Liu, Self-reinforcing and toughening isotactic polypropylene via melt sequential injection molding, Polym. Test. 67 (2018) 183–189.
[20] J. Wang, Z. Du, T. Lian, Extrusion–calendering process of single-polymer composites based on polyethylene, Polym. Eng. Sci. 58 (2018) 2156–2165.
[21] N. Kurokawa, A. Hotta, Thermomechanical properties of highly transparent self-reinforced polylactide composites with electrospun stereocomplex polylactide nanofibers, Polymer 153 (2018) 214–222.
[22] C. Schneider, S. Kazemahvazi, B.P. Russell, D. Zenkert, V.S. Deshpande, Impact response of ductile self-reinforced composite corrugated sandwich beams, Compos. Part B 99 (2016) 121–131.
[23] G. Romhány, C.M. Wu, W.Y. Lai, J. Karger-Kocsis, Fracture behavior and damage development in self-reinforced PET composites assessed by located acoustic emission and thermography: effects of flame retardant and recycled PET, Compos. Sci. Technol. 132 (2016) 76–83.
[24] S. Poulikidou, L. Jerpdal, A. Björklund, M. Åkermo, Environmental performance of self-reinforced composites in automotive applications — case study on a heavy truck component, Mater. Des. 103 (2016) 321–329.
[25] P. Hine, V. Broome, I. Ward, The incorporation of carbon nanofibres to enhance the properties of self reinforced, single polymer composites, Polymer 46 (2005) 10936–10944.
[26] R.J. Foster, M.J. Bonner, I.M. Ward, The use of nano and micron-sized particles to enhance the interlayer adhesion in self-reinforced, single-polymer composites, Compos. Sci. Technol. 71 (2011) 461–465.
[27] V. Beloshenko, Y. Voznyak, A. Voznyak, B. Savchenko, New approach to production of fiber reinforced polymer hybrid composites, Compos. Part B 112 (2017) 22–30.
[28] Y. Swolfs, Y. Meerten, P. Hine, I. Ward, I. Verpoest, L. Gorbatikh, Introducing ductility in hybrid carbon fibre/self-reinforced composites through control of the damage mechanisms, Compos. Struct. 131 (2015) 259–265.
[29] Y. Swolfs, J. Shi, Y. Meerten, P. Hine, I. Ward, I. Verpoest, L. Gorbatikh, The importance of bonding in intralayer carbon fibre/self-reinforced polypropylene hybrid composites, Compos. A 76 (2015) 299–308.
[30] M. Selezneva, Y. Swolfs, A. Katalagarianakis, T. Ichikawa, N. Hirano, I. Taketa, T. Karaki, I. Verpoest, L. Gorbatikh, The brittle-to-ductile transition in tensile and impact behavior of hybrid carbon fibre/self-reinforced polypropylene composites, Compos. A 109 (2018) 20–30.
[31] P.J. Hine, M.J. Bonner, I.M. Ward, Y. Swolfs, I. Verpoest, The influence of the hybridisation configuration on the mechancial properties of hybrid self reinforced polyamide 12/carbon fibre composites, Compos. A 95 (2017) 141–151.
[32] Y. Swolfs, P. De Cuyper, M.G. Callens, I. Verpoest, L. Gorbatikh, Hybridisation of two ductile materials – steel fibre and self-reinforced polypropylene composites, Compos. A 100 (2017) 48–54.
[33] C.N. Rao, A.K. Sood, K.S. Subrahmanyam, A. Govindaraj, Graphene: the new two-dimensional nanomaterial, Angew. Chem. Int. Ed. 48 (2010) 7752–7777.
[34] T. Kuilla, S. Bhadra, D. Yao, N.H. Kim, S. Bose, J.H. Lee, Recent advances in graphene based polymer composites, Prog. Polym. Sci. 35 (2010) 1350–1375.
[35] D. Galpaya, M. Wang, M. Liu, N. Motta, E. Waclawik, C. Yan, Recent advances in fabrication and characterization of graphene-polymer nanocomposites, Graphene 1 (2) (2012) 30–49.

[36] D.G. Papageorgiou, I.A. Kinloch, R.J. Young, Mechanical properties of graphene and graphene-based nanocomposites, Prog. Mater. Sci. 90 (2017) 75–127.
[37] Y. Li, S. Wang, Q. Wang, M. Xing, A comparison study on mechanical properties of polymer composites reinforced by carbon nanotubes and graphene sheet, Compos. Part B 133 (2018) 35–41.
[38] A. Amash, P. Zugenmaier, Morphology and properties of isotropic and oriented samples of cellulose fibre-polypropylene composites, Polymer 41 (2000) 1589–1596.
[39] F.A. Hoor, J. Morshedian, S. Ahmadi, M. Rakhshanfar, A. Bahramzadeh, Effect of graphene nanosheets on the morphology, crystallinity, and thermal and electrical properties of super tough polyamide 6 using SEBS compounds, J. Chemother. 819580 (2015).
[40] Y. Li, J. Zhu, S. Wei, J. Ryu, L. Sun, Z. Guo, Poly(propylene)/graphene nanoplatelet nanocomposites: melt rheological behavior and thermal, electrical, and electronic properties, Macromol. Chem. Phys. 212 (2011) 1951–1959.
[41] Y.-S. Jun, J.G. Um, G. Jiang, A. Yu, A study on the effects of graphene nano-platelets (GnPs)sheet sizes from a few to hundred microns on the thermal, mechanical, and electrical properties of polypropylene (PP)/GnPs composites, Express Polym Lett 12 (2018) 885–897.
[42] J. Li, P. Xiao, H. Li, Y. Zhang, F. Xue, B. Luo, S. Huang, Y. Shang, H. Wen, J.C. Christiansen, D. Yu, S. Jiang, Crystalline structures and crystallization behaviors of poly(l-lactide) in poly(l-lactide)/graphene nanosheet composites, Polym. Chem. 6 (2015) 3988–4002.
[43] J. Wang, J. Chen, P. Dai, S. Wang, D. Chen, Properties of polypropylene single-polymer composites produced by the undercooling melt film stacking method, Compos. Sci. Technol. 107 (2015) 82–88.
[44] Y. Swolfs, Q. Zhang, J. Baets, I. Verpoest, The influence of process parameters on the properties of hot compacted self-reinforced polypropylene composites, Compos. A 65 (2014) 38–46.
[45] S. Bastida, J.I. Eguiazábal, M. Gaztelumendi, J. Nazábal, On the thickness dependence of the modulus of elasticity of polymers, Polym. Test. 17 (1998) 139–145.
[46] J. Liang, Q. Du, G.C.-P. Tsui, C.-Y. Tang, Tensile properties of graphene nano-platelets reinforced polypropylene composites, Compos. Part B 95 (2016) 166–171.
[47] S.R. Ahmad, C. Xue, R.J. Young, The mechanisms of reinforcement of polypropylene by graphene nanoplatelets, Mater. Sci. Eng. B 216 (2017) 2–9.
[48] C.-L. Huang, C.-W. Lou, C.-F. Liu, C.-H. Huang, X.-M. Song, J.-H. Lin, Polypropylene/graphene and polypropylene/carbon fiber conductive composites: mechanical, crystallization and electromagnetic properties, Appl. Sci. 5 (2015) 1196–1210.
[49] M.A. Milani, D. González, R. Quijada, N.R.S. Basso, M.L. Cerrada, D.S. Azambuja, G.B. Galland, Polypropylene/graphene nanosheet nanocomposites by in situ polymerization: synthesis, characterization and fundamental properties, Compos. Sci. Technol. 84 (2013) 1–7.
[50] P. Song, Z. Cao, Y. Cai, L. Zhao, Z. Fang, S. Fu, Fabrication of exfoliated graphene-based polypropylene nanocomposites with enhanced mechanical and thermal properties, Polymer 52 (2011) 4001–4010.
[51] Y.S. Yun, Y.H. Bae, D.H. Kim, J.Y. Lee, I.J. Chin, H.J. Jin, Reinforcing effects of adding alkylated graphene oxide to polypropylene, Carbon 49 (2011) 3553–3559.
[52] K. Wakabayashi, P.J. Brunner, J.I. Masuda, S.A. Hewlett, J.M. Torkelson, Polypropylene-graphite nanocomposites made by solid-state shear pulverization: effects of significantly exfoliated, unmodified graphite content on physical, mechanical and electrical properties, Polymer 51 (2010) 5525–5531.